Sciencexpress Research Article

Fermi Observations of High-Energy Gamma-Ray Emission from GRB 080916C

The Fermi LAT and Fermi GBM Collaborations*

*The full list of authors and affiliations is presented at the end of this paper.

Gamma-ray bursts (GRBs) are highly energetic explosions signaling the death of massive stars in distant galaxies. The Gamma-Ray Burst Monitor and Large Area Telescope onboard the Fermi Observatory together record GRBs over a broad energy range spanning about seven decades of gamma-ray energy. In September 2008, Fermi observed the exceptionally luminous GRB 080916C, with the largest apparent energy release yet measured. The high-energy gamma rays are observed to start later and persist longer than the lower energy photons. A simple spectral form fits the entire GRB spectrum, providing strong constraints on emission models. The known distance of the burst enables placing lower limits on the bulk Lorentz factor of the outflow and on the quantum gravity mass.

Gamma-ray bursts (GRBs) are the most luminous explosions in the universe and are leading candidates for the origin of ultra high-energy cosmic rays (UHECRs). Prompt emission from GRBs from ~ 10 keV to ~ 1-5 MeV has usually been detected but, occasionally photons above 100 MeV have been detected by the Energetic Gamma-Ray Experiment Telescope (EGRET) (*1*), and more recently by Astro-rivelatore Gamma a Immagini LEggero (AGILE) (*2*). Observations of gamma rays with energies > 100 MeV are particularly prescriptive because they constrain the source environment and help understand the underlying energy source. Although there have been observations of photons above 100 MeV (*3*–*5*), it has not been possible to distinguish competing interpretations of the emission (*6*–*8*). The *Fermi* Gamma-ray Space Telescope, launched on 11 June 2008, provides broad energy coverage and high GRB sensitivities through the Gamma-ray Burst Monitor (GBM) and the Large Area Telescope (LAT) (*9*). The GBM consists of 12 sodium iodide (NaI) detectors which cover the energy band between 8 keV and 1 MeV, and two bismuth germanate (BGO) scintillators which are for the energy band between 150 keV and 40 MeV. The LAT is a pair conversion telescope with the energy coverage from below 20 MeV to more than 300 GeV (supporting online text). In this paper, we report detailed measurements of gamma-ray emission from the GRB 080916C detected by the GBM and LAT.

Observations. At 00:12:45.613542 UT (T_0) on September 16 2008 the GBM Flight Software triggered on GRB 080916C. The GRB produced large signals in 9 of the 12 NaI detectors and in one of the two BGO detectors. Analysis of the data on the ground localized the burst to a Right Ascension (RA) = $08^h07^m12^s$, Declination (Dec) = $-61^\circ18'00''$ (*10*), with an uncertainty of 2.8° at 68% confidence level (C.L.).

At the time of the trigger, the GRB was located ~ 48° from the LAT boresight and on-ground analysis revealed a bright source consistent with the GRB location. Using the events collected during the first 66 s after T_0, within 20° around the GBM burst position, the LAT provided a localization of RA = $07^h59^m31^s$, Dec. = $-56^\circ35'24''$ (*11*) with a statistical uncertainty of 0.09° at 68% C.L. (0.13° at 90% C.L.) and a systematic uncertainty smaller than ~ 0.1° (see Movie S1).

Follow-up X-ray and optical observations revealed a fading source at RA = $07^h59^m23.24^s$, Dec. = $-56^\circ38'16.8''$ (±1.9" at 90% C.L.) (*12*) by Swift/X-Ray Telescope (XRT) and RA = $07^h59^m23.32^s$, Dec. = $-56^\circ38'18.0''$ (±0.5")) (*13*, *14*) by Gamma-Ray Burst Optical/Near-Infrared Detector (GROND), respectively, consistent with the LAT localization within the estimated uncertainties. GROND determined the redshift of this source to be $z = 4.35 \pm 0.15$ (*15*). The afterglow was also observed in the near-infrared band by the Nagoya-SAAO 1.4 m telescope (IRSF) (*16*). The X-ray lightcurve of the afterglow from T_0+61 ks to T_0+1306 ks shows two temporal breaks at about 2 and 4 days after the trigger (*17*). The lightcurves before, between and after the breaks can be fit with a power-law function with decay indices ~ –2.3, ~ –0.2 and ~ –1.4, respectively.

The lightcurve of GRB 080916C, as observed with *Fermi* GBM and LAT, is shown in Fig.1. The total number of LAT counts after background subtraction in the first 100 s after the trigger was > 3000. For most of the low-energy events, however, extracting reliable directional and energy information was not possible. After we applied standard selection cuts (*9*) for transient sources with energies greater than 100 MeV and directions compatible with the burst location, 145 events remained (panel 4), and 14 events had energies > 1 GeV.

Because of the energy-dependent temporal structure of the lightcurve, we divided the lightcurve into five time intervals

(a,b,c,d,e) delineated by the vertical lines (Fig.1). The GRB lightcurve at low energy has two bright peaks, one between 0 and 3.6 s after the trigger (interval `a'), and one between 3.6 and 7.7 s (interval `b'). The two peaks are distinct in the BGO lightcurve, but less so in the NaI. In the LAT detector the first peak is not significant though the lightcurve shows evidence of activity in time interval (a), mostly in events below 100 MeV. Above 100 MeV, peak (b) is prominent in the LAT lightcurve. Interval (c) coincides with the tail of the main pulse, and the last two intervals reflect temporal structure in the NaI lightcurve and have been chosen to provide enough statistics in the LAT energy band for spectral analysis. The highest energy photon was observed during interval (d): $E_h = 13.22^{+0.70}_{-1.54}$ GeV. Most of the emission in peak (b) shifts toward later times as the energy increases (inset).

Spectral analysis. We performed simultaneous spectral fits of the GBM and LAT data for each of the five time bins described above and shown in Fig. 1. GBM NaI data from detectors 3 and 4 were selected from 8 keV to 1.0 MeV, as well as BGO detector 0 data from 0.26 to 40 MeV. LAT photons were selected using the ``transient'' event class (*9*) for the energies from 100 MeV to 200 GeV. This event class provides the largest effective area and highest background rates among the LAT standard event classes, which is appropriate for bright sources with small backgrounds like this burst. This combination of the GBM and LAT data results in joint spectral fits using forward-folding techniques covering over seven decades of energy (supporting online text).

The spectra of all five time intervals are well fit by the empirical Band function (*18*) which smoothly joins low- and high-energy power laws. The first time interval, with a relative paucity of photons in the LAT, also has the most distinct spectral parameter values. The low-energy photon index α is larger (indicating harder emission) and the high-energy photon index β is smaller (indicating softer emission) - consistent with the small number of LAT photons observed at this time. After the first interval there was no significant evolution in either α or β, as is evident in Fig. 3. In contrast, E_{peak}, the energy at which the energy emission peaks in the sense of energy per photon energy decade, evolved from the first time bin to reach its highest value in the second time bin, then softened through the remainder of the GRB. The higher E_{peak} and overall intensity of interval (b), combined with the hard value of β that is characteristic of the later intervals, are the spectral characteristics that lead to the emission peaking in the LAT lightcurve (Fig. 1). The spectrum of interval (b) with a Band function fit is shown in Fig. 2. Comparing the parameters of this interval to the ensemble of EGRET burst detections: the flux at around 1 MeV and β are similar to those for GRB 910503 and E_{peak} resembles that for GRB 910814 (*19*).

We searched for deviations from the Band function, such as an additional component at high energies (*5*). Three photons in the fourth time bin had energies above 6 GeV. We tried modeling these high-energy photons with a power law as an additional high-energy spectral component. Compared to the null hypothesis that the data originated from a simple Band GRB function, adding the additional power-law component resulted in a probability of 1% that there was no additional spectral component for this time bin; with five time bins, this is not strong evidence for any additional component. Our sensitivity to higher-energy photons may be reduced at $z \sim 4.35$ through absorption by Extragalactic Background Light (EBL). Because the effect of various EBL models ranges widely, from leaving the single time bin spectral-fit probability of an extra component unchanged (*20*) to decreasing the spectral-fit plausiblity of its absence to 0.03% (*21*), we cannot use EBL absorption effects in our estimation of significance.

Long-lived emissions. Although the lightcurves shown in Fig. 1 indicate that during interval (e) the spiky structures typical of prompt GRB emission appear to be dying out, the emission persisted in some of the GBM NaI detectors at a low level out to nearly T_0 + 200 s. The lack of pulse structure and the background-limited nature of the NaI detectors make this emission difficult to associate conclusively with the GRB, but the excess above background in the 12 NaI detectors occurred in the ratios expected for the geometry of the detectors relative to the burst direction. In addition, this type of low-level, extended emission is a known phenomenon in at least some long GRBs (*22*), so we associate it with the GRB and fit the spectrum with a power-law index of -1.92 ± 0.21. Emission beyond T_0 + 200 s fell below the threshold of the GBM detectors. Because of much lower instrumental backgrounds in the LAT, a high-energy decaying component might be seen for a longer time. The most suitable class to study faint sources with minimum backgrounds (``diffuse'') was used to select events within 15° of the GROND localization coordinates between T_0+100 s and T_0+1400 s, which were then examined for possible connection with the GRB source. The interval up to T_0+200 s was treated separately for correlation with contemporaneous data from the GBM. The upper bound was chosen because after T_0+1400 s, the GRB off-axis angle increased from 50° to 62° resulting in decreased effective area.

We performed unbinned maximum likelihood fits of a power-law spectral function for a point source at the GROND-determined burst location in these two time intervals. Contributions from instrumental, Galactic, extragalactic components were included in the fit, as well as the bright source Vela (which is located 13° from the GRB). Both time intervals show the presence of significant flux. For the final time interval, T_0+200 to T_0+1400 s, the fit yields a

flux of $(6.4\pm2.5)\times10^{-6}$ γ cm^{-2} s^{-1} for $E > 100$ MeV with a power-law photon index of −2.8 ±0.5 at a significance of 5.6σ. The fitting process does not assign individual photons to particular sources; it predicts, however, that 10.4 of the fitted photons originated from the GRB. If the position of the point source is left free instead of fixed to the GROND localization, the fit yields a source position of RA = $07^h57^m33^s$, Dec. = $-57^{\circ}00'00''$ with an uncertainty of 0.51° at 90% C.L. This location is 0.45° from, and in agreement with, the GROND GRB position. To solidify the association of this extended emission with the GRB, we performed the same source detection procedure for data from T_0–900 s to T_0 and no emission was observed. A search for emission beyond T_0+1400 s was also fruitless.

We therefore associate this long-lived component with the GRB and include it as a sixth and seventh time interval for comparison with the early-time emission (Fig. 4). In the LAT data, a constantly declining high-energy flux with a power-law decay index of −1.2±0.2 is seen throughout T_0+1400 s (red points, Fig. 4). On the other hand, the flux in the GBM band shows a slower decay initially and an apparent break in the lightcurve at ~ T_0+55 s. The power-law decay indices are approximately −0.6 and −3.3 before and after the break, respectively. Previous reports (*3*, *5*) have provided tantalizing clues that distinct high-energy components may be a feature of some GRBs.

Interpretation. The *Fermi* observations of GRB 080916C show that the event energy spectra up to ~ 100 s are consistent with a single model (Band function), suggesting that a single emission mechanism dominates.

Between 10 keV and 10 GeV in the observer's frame, we measure a fluence $f = 2.4\times10^{-4}$ ergs cm^{-2} which gives at z = 4.35 an apparent isotropic energy release for a standard cold dark matter cosmology with cosmological constant Ω_Λ = 0.73, Ω_m = 0.27, and a Hubble's constant of 71 km s^{-1} Mpc^{-1} of $E_{iso} \cong 8.8\times10^{54}$ ergs (supporting online text). This is ~ 4.9 times the Solar rest energy, and therefore strongly suggests on energetic grounds, for any stellar mass progenitor, that the GRB outflow powering this emission occupied only a small fraction ($<\sim10^{-2}$) of the total solid angle, and was collimated into a narrow jet. A comparison with the previous highest measured $E_{iso} = 2.0\times10^{54}$ from 20 keV to 2 MeV shows the fluence and E_{iso} for GRB 080916C in this energy range are 1.2×10^{-4} ergs cm^{-2} and 4.3×10^{54} ergs, respectively. This earlier burst, GRB 990123 (*23*), was detected up to ≈ 20 MeV by the EGRET TASC instrument.

High-energy γ rays from such intense regions can be strongly attenuated by lower-energy photons via pair production. The pair-production opacity can be reduced if the emission region is moving toward us at highly relativistic speeds - a relativistic jet with Lorentz factor Γ also explains the intensity and rapid variability of GRB γ rays (*24*–*28*). The observed correlated variability of the GBM and LAT emissions indicates that photons formed co-spatially, with the lower-energy (GBM) photons providing target photons that can interact with higher energy γ rays to produce electron-positron pairs. Using the Band function as the target radiation field and setting to unity the optical depth $\tau_{\gamma\gamma}$ to γ-ray pair production attenuation of the highest-energy observed photon, we calculate Γ_{min}, the minimum bulk Lorentz factor (supporting online text) (Fig.5). For $z = 4.35$, we obtain Γ_{min} = 608 ±15 and 887 ±21 in time bins d and b, respectively. For a spherical emitting shell of radius R, the observed variability time Δt and Γ_{min} can be used to set a lower limit on the emission radius, $R > \Gamma_{min}^2\, c\Delta t/(1+z) = 8.9\times10^{15}(\Gamma_{min}/890)^2(\Delta t/2\ s)(5.35/(1+z))$ cm. Similarly large prompt emission radii were inferred for other GRBs on different grounds (*29*, *30*).

The delayed onset of the GRB 080916C LAT pulse, which coincides with the rise of the second peak in the GBM light curve (see Fig.1) suggests a common origin, in a region spatially distinct from the first GBM pulse. In the framework of the internal-shocks model for the prompt emission of GRBs (*27*, *28*), where intermittent winds of relativistic plasma are ejected by a newly-formed black hole and collide to form shocks and accelerate particles, the two emission regions could arise from two different pairs of colliding shells, with variations in physical conditions leading to nonthermal electrons with different spectral hardnesses.

An alternative explanation for the delayed onset of the LAT emission is that a volume becomes filled with radiation that attenuates the high-energy photons until a later time when the emitting region expands and becomes optically thin. A γγ pair-production opacity effect would, however, produce a high-energy spectral softening or cutoff, whereas in all cases the combined GBM/LAT data are well fit with simple models using the Band parameterization. Moreover, internal γ-ray opacity models predict that high-energy photons should also be detected in the rising portion of the GBM emission while they can still escape the source, before the increased photon density attenuates the γ rays (*31*). Finally, in hadronic models associated with UHECR and high-energy neutrino production, the delay of the LAT emission could be a consequence of the time needed to accelerate protons or ions to energies where they can radiate by photopion or proton synchrotron radiation and generate an electromagnetic cascade (*32*–*34*). It is, however, unclear whether such models can reproduce the observed 10 keV to 10 GeV spectrum.

Before our observations, a high-energy (100 MeV - GeV) tail was observed most clearly from GRB 940217 (*3*) in observations by EGRET. The continuous high-energy tail in GRB 080916C could be due to the delayed arrival of the SSC emission in the GeV energy band during the afterglow phase (*35*). The observations, however, lack the predicted spectral

hardening expected as the GeV emission changes from prompt synchrotron to afterglow SSC radiation. The LAT high-energy tail could also result from angle-dependent scattering effects (*36*), or from cascades induced by ultrarelativistic ions accelerated in GRBs (*8*).

The lack of two distinct emission components in the spectra up to ~ 10 GeV throughout the burst is compatible with a nonthermal synchrotron origin of the radiation. This is the favored emission mechanism at keV - MeV energies (*27*), and can indeed reach ~ 30(Γ/1000)(5.35/(1+z)) GeV (*37*). Nonthermal synchrotron radiation should, however, be accompanied by a synchrotron self-Compton (SSC) spectral component produced from electrons that Compton upscatter their synchrotron photons to γ-ray energies potentially in the LAT energy band. The apparent lack of an SSC component indicates that the magnetic energy density is much higher than the electron energy density (supporting online text), or that the SSC νF_ν spectrum peaks at >> 10 GeV and thus cannot be detected, which requires a typical electron Lorentz factor $\gamma_m \sim (E_{\rm peak}{}^{\rm SSC}/E_{\rm peak}{}^{\rm syn})^{1/2} >> 100$.

In addition to these considerations, sensitivity to a high-energy additional spectral component is reduced because Extragalactic Background Light (EBL) can absorb high-energy photons via pair-production interactions. In GRB 080916C we observed neither a spectral cutoff that might be a signature of EBL, nor does the observation of a 13.2 GeV photon discriminate between EBL models (supporting online text). Moreover, if EBL is hiding an additional spectral component we may be underestimating the energetics of GRB 080916C.

The high photon energies and large distance of GRB 080916C can test a prediction of some quantum gravity models that energy dispersion exists in the speed of photons - high-energy photons traveling slower and therefore arriving to us later than low-energy photons (*38*). In the linear approximation, the difference in the arrival times Δt is proportional to the ratio of photon energy difference to the quantum gravity mass, $\Delta E/M_{\rm QG}$, and depends on the distance the photons traveled. The arrival time of the $13.22^{+0.70}_{-1.54}$ GeV photon relative to T_0, $t = 16.54$ s, is a conservative upper limit on its Δt relative to ~ MeV photons, and implies a robust lower limit on the quantum gravity mass, $M_{\rm QG} > 1.3 \times 10^{18}$ GeV/c^2 (Supporting online text). We have used the low-end of the 1σ confidence intervals of both z and E_h in calculationg $M_{\rm QG}$. This lower limit is only one order of magnitude smaller than the Planck mass, 1.22×10^{19} GeV/c^2.

In the first five months since triggering was enabled on 14 July 2008, GBM triggered on 58 GRBs within the LAT field-of view: besides GRB 080916C (discussed here) two additional events were also seen with the LAT. The first was GRB 080825C (*39*), and the third was GRB 081024B, the first short GRB observed with the LAT (*40*, *41*). Fig. 6 shows the LAT (100 MeV - 10 GeV) versus the GBM (20 keV - 2 MeV) fluences measured during the entire duration of each event. GRB 080916C stands out in both instruments, enabling better statistics in its spectral and timing analyses. Moreover, unlike the other two events, GRB 080916C has a redshift measurement, enabling determinations of lower limits for the bulk Lorentz factor of its ejecta and of the quantum gravity mass $M_{\rm QG}$.

Fig. 6 raises questions about the relation between the low and high energy emission. In no case have we detected a high-energy excess that would imply a distinct spectral component such as an SSC peak. The constraints are, however, weaker for GRBs 081024B and 080825C which have fewer detected counts with which we could fit additional components. We observe in all three GRBs a delay in the onset of the LAT (E > 100 MeV) photons with respect to the lower energy GBM photons. This trend is an important clue for unraveling the GRB phenomenon.

References and Notes

1. B. L. Dingus, *Astrophys. Space Sci.* **231**, 187 (1995).
2. A. Giuliani *et al.*, *Astron. Astrophys.* in press; arXiv:0809.1230 (2008).
3. K. Hurley *et al.*, *Nature* **372**, 652 (1994).
4. D. N. Wren, D. L. Bertsch, S.Ritz, *Astrophys. J.* **574**, L47 (2002).
5. M. M. Gonźalez *et al.* , *Nature* **424**, 749 (2003).
6. J. Granot, D. Guetta, *Astrophys. J.* **598**, L11 (2003).
7. J.Katz, *Astrophys. J.* **432**, L27 (1994).
8. C. D. Dermer, A. Atoyan, *New J. Phys.* **8**, 122 (2006).
9. W. B. Atwood *et al.*, arXiv:0902.1089 (2008).
10. A. Goldstein, A.vander Horst, *GCN Circular 8245* (2008).
11. H. Tajima *et al.*, *GCN Circular 8246* (2008).
12. M. Perri *et al.*, *GCN Circular 8261* (2008).
13. C. Clemens*et al.*, *GCN Circular 8257* (2008).
14. C. Clemens*et al.*, *GCN Circular 8272* (2008).
15. J. Greiner *et al.*, arXiv:0902.0761 (2009).
16. T. Nagayama *et al.*, *GCN Circular 8274* (2008).
17. G. Stratta*et al.*, *GCN Report 166.1* (2008).
18. D. Band *et al.*, *Astrophys. J.* **413**, 281 (1993).
19. M. Baring, *Astrophys. J.* **650**, 1004 (2006).
20. S. Razzaque, C. D. Dermer, J. D. Finke, astro-ph 0807.4294 (2008).
21. F. W. Stecker, M. A. Malkan, S. T. Scully, *Astrophys.J.* **648**, 774 (2006).
22. V. Connaughton, *Astrophys. J.* **567**, 1028 (2002).
23. M. S. Briggs, *et al.* , *Astrophys.J.* **524**, 82 (1999).
24. J. H. Krolik, E. A. Pier, *Astrophys. J.* **373**, 277 (1991).
25. E. E. Fenimore, R. I. Epstein, C. Ho, *Astron. Astrophys. Suppl. Ser.* **97**, 59 (1993).
26. Y. Lithwick, R. Sari, *Astrophys. J.* **555**, 540 (2001).

27 P. Mészáros, *Annu. Rev. Astron. Astrophys.* **40**, 137 (2002).
28. T. Piran, *Phys. Rep.* **314**, 575 (1999).
29. P. Kumar *et al.*, *MNRAS* **376**, L57 (2007).
30. J. L. Racusin, *Nature* **455**, 183 (2008).
31. J. Granot, J. Cohen-Tanugi, E. do Couto e Silva, *Astrophys. J.* **677**, 92 (2008).
32. J. P. Rachen, P. Mészáros, *Phys. Rev. D* **58**, 123005 (1998).
33. C. D. Dermer, *Astrophys. J.* **574**, 65 (2002).
34. S. Razzaque, P. Mészáros, E. Waxman, *Mod. Phys. Lett. A* **20**, 2351 (2005).
35. R. Sari, A. A. Esin, *Astrophys. J.* **548**, 787 (2001).
36. X. Y. Wang, Z. Li, P. Mészáros, *Astrophys. J.* **641**, L89 (2006).
37. A. A. Pe'er, E. Waxman, *Astrophys. J.* **613**, 448 (2004).
38. G. Amelino-Camelia *et al.*, *Nature* **393**, 763 (1998).
39. A. Bouvier *et al.*, *GCN Circular 8183* (2008).
40. N. Omodei, *GCN Circular 8407* (2008).
41. V. Connaughton, M. S. Briggs, *GCN Circular 8408* (2008).
42. A. A. Abdo, J. Finke, and S. Razzaque are National Research Council Research Associates. A. J. van der Horst is a NASA Postdoctoral Program Fellow. The *Fermi* LAT Collaboration acknowledges the support of a number of agencies and institutes. These include the National Aeronautics and Space Administration and the Department of Energy in the United States, the Commissariat à l'Energie Atomique and the Centre National de la Recherche Scientifique / Institut National de Physique Nucléaire et de Physique des Particules in France, the Agenzia Spaziale Italiana and the Istituto Nazionale di Fisica Nucleare in Italy, the Ministry of Education, Culture, Sports, Science and Technology (MEXT), High Energy Accelerator Research Organization (KEK) and Japan Aerospace Exploration Agency (JAXA) in Japan, and the K. A. Wallenberg Foundation, the Swedish Research Council and the Swedish National Space Board in Sweden. JC is Royal Swedish Academy of Sciences Research fellow supported by a grant from the K. A. Wallenberg foundation. The *Fermi* GBM Collaboration acknowledges the support of NASA in the United States and DRL in Germany, and thanks Lisa Gibby, Al English and Fred Kroeger.

Supporting Online Material

www.sciencemag.org/cgi/content/full/1169101/DC1
SOM Text
Figs. S1 to S7
Movie S1

27 November 2008; accepted 11 February 2009
Published online 19 February 2009;
10.1126/science.1169101
Include this information when citing this paper.

***List of authors and affiliations:** A. A. Abdo[1,2], M. Ackermann[3], M. Arimoto[4], K. Asano[4], W. B. Atwood[5], M. Axelsson[6,7], L. Baldini[8], J. Ballet[9], D. L. Band[10,11], G. Barbiellini[12,13], M. G. Baring[14], D. Bastieri[15,16], M. Battelino[6,17], B. M. Baughman[18], K. Bechtol[3], F. Bellardi[8], R. Bellazzini[8], B. Berenji[3], P. N. Bhat[19], E. Bissaldi[20], R. D. Blandford[3], E. D. Bloom[3], G. Bogaert[26], J. R. Bogart[3], E. Bonamente[21,22], J. Bonnell[11], A. W. Borgland[3], A. Bouvier[3], J. Bregeon[8], A. Brez[8], M. S. Briggs[19,23], M. Brigida[24,25], P. Bruel[26], T. H. Burnett[27], D. Burrows[28], G. Busetto[15,16], G. A. Caliandro[24,25], R. A. Cameron[3], P. A. Caraveo[29], J. M. Casandjian[9], M. Ceccanti[8], C. Cecchi[21,22], A. Celotti[30], E. Charles[3], A. Chekhtman[31,2], C. C. Cheung[11], J. Chiang[3], S. Ciprini[21,22], R. Claus[3], J. Cohen-Tanugi[32], L. R. Cominsky[33], V. Connaughton[19], J. Conrad[6,17,34], L. Costamante[3], S. Cutini[35], M. DeKlotz[36], C. D. Dermer[2,23], A. de Angelis[37], F. de Palma[24,25], S. W. Digel[3], B. L. Dingus[38], E. do Couto e Silva[3], P. S. Drell[3], R. Dubois[3], D. Dumora[39,40], Y. Edmonds[3], P. A. Evans[41], D. Fabiani[8], C. Farnier[32], C. Favuzzi[24,25], J. Finke[1,2], G. Fishman[42], W. B. Focke[3], M. Frailis[37], Y. Fukazawa[43], S. Funk[3], P. Fusco[24,25], F. Gargano[25], D. Gasparrini[35], N. Gehrels[11,44], S. Germani[21,22], B. Giebels[26], N. Giglietto[24,25], P. Giommi[35], F. Giordano[24,25], T. Glanzman[3], G. Godfrey[3], A. Goldstein[19], J. Granot[45], J. Greiner[20], I. A. Grenier[9], M.-H. Grondin[39,40], J. E. Grove[2], L. Guillemot[39,40], S. Guiriec[32], G. Haller[3], Y. Hanabata[43], A. K. Harding[11], M. Hayashida[3], E. Hays[11], J. A. Hernando Morata[46], A. Hoover[38], R. E. Hughes[18], G. Jóhannesson [3], A. S. Johnson[3], R. P. Johnson[5], T. J. Johnson[11,44], W. N. Johnson[2], T. Kamae[3], H. Katagiri[43], J. Kataoka[4], A. Kavelaars[3], N. Kawai[47,4], H. Kelly[3], J. Kennea[28], M. Kerr[27], R. M. Kippen[38], J. Knödlseder [48], D. Kocevski[3], M. L. Kocian[3], N. Komin[9,32], C. Kouveliotou[42], F. Kuehn[18], M. Kuss[8], J. Lande[3], D. Landriu[9], S. Larsson[6,34], L. Latronico[8], C. Lavalley[32], B. Lee[49], S.-H. Lee[3], M. Lemoine-Goumard[39,40], G. G. Lichti[20], F. Longo[12,13], F. Loparco[24,25], B. Lott[39,40], M. N. Lovellette[2], P. Lubrano[21,22], G. M. Madejski[3], A. Makeev[31,2], B. Marangelli[24,25], M. N. Mazziotta[25], S. McBreen[20,50], J. E. McEnery[11], S. McGlynn[6,17], C. Meegan[42], P. Mészáros [28], C. Meurer[6,34], P. F. Michelson[3], M. Minuti[8], N. Mirizzi[24,25], W. Mitthumsiri[3], T. Mizuno[43], A. A. Moiseev[10], C. Monte[24,25], M. E. Monzani[3], E. Moretti[12,13], A. Morselli[51], I. V. Moskalenko[3], S. Murgia[3], T. Nakamori[4], D. Nelson[3], P. L. Nolan[3], J. P. Norris[52], E. Nuss[32], M. Ohno[53], T. Ohsugi[43], A. Okumura[54], N. Omodei[8], E. Orlando[20], J. F. Ormes[52], M. Ozaki[53], W. S. Paciesas[19], D. Paneque[3], J. H. Panetta[3], D. Parent[39,40], V. Pelassa[32], M. Pepe[21,22], M. Perri[35], M. Pesce-Rollins[8], V. Petrosian[3], M. Pinchera[8], F. Piron[32], T. A. Porter[5], R. Preece[42], S. Rainò [24,25], E. Ramirez-Ruiz[55], R. Rando[15,16], E. Rapposelli[8], M. Razzano[8], S. Razzaque[1,2], N. Rea[56,57], A. Reimer[3], O. Reimer[3], T. Reposeur[39,40], L. C. Reyes[58], S. Ritz[11,44], L. S. Rochester[3], A. Y. Rodriguez[57], M. Roth[27], F. Ryde[6,17], H. F.-W. Sadrozinski[5], D. Sanchez[26], A. Sander[18], P. M. Saz Parkinson[5], J. D. Scargle[59],

T. L. Schalk[5], K. N. Segal[11], C. Sgrò[8], T. Shimokawabe[4], E. J. Siskind[60], D. A. Smith[39,40], P. D. Smith[18], G. Spandre[8], P. Spinelli[24,25], M. Stamatikos[11], J.-L. Starck[9], F. W. Stecker[11], H. Steinle[20], T. E. Stephens[11], M. S. Strickman[2], D. J. Suson[61], G. Tagliaferri[62], H. Tajima[3,23], H. Takahashi[43], T. Takahashi[53], T. Tanaka[3], A. Tenze[8], J. B. Thayer[3], J. G. Thayer[3], D. J. Thompson[11], L. Tibaldo[15,16], D. F. Torres[63,57], G. Tosti[21,22], A. Tramacere[64,3], M. Turri[3], S. Tuvi[3], T. L. Usher[3], A. J. van der Horst[42,65], L. Vigiani[8], N. Vilchez[48], V. Vitale[51,66], A. von Kienlin[20], A. P. Waite[3], D. A. Williams[5], C. Wilson-Hodge[42], B. L. Winer[18], K. S. Wood[2], X. F. Wu[67,28,68], R. Yamazaki[43], T. Ylinen[69,6,17], M. Ziegler[5]

[1]National Research Council Research Associate [2]Space Science Division, Naval Research Laboratory, Washington, DC 20375 [3]W. W. Hansen Experimental Physics Laboratory, Kavli Institute for Particle Astrophysics and Cosmology, Department of Physics and SLAC National Laboratory, Stanford University, Stanford, CA 94305 [4]Department of Physics, Tokyo Institute of Technology, Meguro City, Tokyo 152-8551, Japan [5]Santa Cruz Institute for Particle Physics, Department of Physics and Department of Astronomy and Astrophysics, University of California at Santa Cruz, Santa Cruz, CA 95064 [6]The Oskar Klein Centre for Cosmo Particle Physics, AlbaNova, SE-106 91 Stockholm, Sweden [7]Department of Astronomy, Stockholm University, SE-106 91 Stockholm, Sweden [8]Istituto Nazionale di Fisica Nucleare, Sezione di Pisa, I-56127 Pisa, Italy [9]Laboratoire AIM, CEA-IRFU/CNRS/ Université Paris Diderot, Service d'Astrophysique, CEA Saclay, 91191 Gif sur Yvette, France [10]Center for Research and Exploration in Space Science and Technology (CRESST), NASA Goddard Space Flight Center, Greenbelt, MD 20771 [11]NASA Goddard Space Flight Center, Greenbelt, MD 20771 [12]Istituto Nazionale di Fisica Nucleare, Sezione di Trieste, I-34127 Trieste, Italy [13]Dipartimento di Fisica, Università di Trieste, I-34127 Trieste, Italy [14]Rice University, Department of Physics and Astronomy, MS-108, P. O. Box 1892, Houston, TX 77251, USA [15]Istituto Nazionale di Fisica Nucleare, Sezione di Padova, I-35131 Padova, Italy [16]Dipartimento di Fisica "G. Galilei", Università di Padova, I-35131 Padova, Italy [17]Department of Physics, Royal Institute of Technology (KTH), AlbaNova, SE-106 91 Stockholm, Sweden [18]Department of Physics, Center for Cosmology and Astro-Particle Physics, The Ohio State University, Columbus, OH 43210 [19]University of Alabama in Huntsville, Huntsville, AL 35899 [20]Max-Planck Institut für extraterrestrische Physik, 85748 Garching, Germany [21]Istituto Nazionale di Fisica Nucleare, Sezione di Perugia, I-06123 Perugia, Italy [22]Dipartimento di Fisica, Università degli Studi di Perugia, I-06123 Perugia, Italy [23]Corresponding authors: M. S. Briggs, michael.briggs@nasa.gov; H. Tajima, htajima@slac.stanford.edu; C. D. Dermer, charles.dermer@nrl.navy.mil. [24]Dipartimento di Fisica "M. Merlin" dell'Università e del Politecnico di Bari, I-70126 Bari, Italy [25]Istituto Nazionale di Fisica Nucleare, Sezione di Bari, 70126 Bari, Italy [26]Laboratoire Leprince-Ringuet, École polytechnique, CNRS/IN2P3, Palaiseau, France [27]Department of Physics, University of Washington, Seattle, WA 98195-1560 [28]Pennsylvania State University, 525 Davey Laboratory, University Park, PA 16802 [29]INAF-Istituto di Astrofisica Spaziale e Fisica Cosmica, I-20133 Milano, Italy [30]Scuola Internazionale Superiore di Studi Avanzati (SISSA), 34014 Trieste, Italy [31]George Mason University, Fairfax, VA 22030 [32]Laboratoire de Physique Théorique et Astroparticules, Université Montpellier 2, CNRS/IN2P3, Montpellier, France [33]Department of Physics and Astronomy, Sonoma State University, Rohnert Park, CA 94928-3609 [34]Department of Physics, Stockholm University, AlbaNova, SE-106 91 Stockholm, Sweden [35]Agenzia Spaziale Italiana (ASI) Science Data Center, I-00044 Frascati (Roma), Italy [36]Stellar Solutions Inc., 250 Cambridge Avenue, Suite 204, Palo Alto, CA 94306 [37]Dipartimento di Fisica, Università di Udine and Istituto Nazionale di Fisica Nucleare, Sezione di Trieste, Gruppo Collegato di Udine, I-33100 Udine, Italy [38]Los Alamos National Laboratory, Los Alamos, NM 87545, USA [39]CNRS/IN2P3, Centre d'Études Nucléaires Bordeaux Gradignan, UMR 5797, Gradignan, 33175, France [40]Université de Bordeaux, Centre d'Études Nucléaires Bordeaux Gradignan, UMR 5797, Gradignan, 33175, France [41]Department of Physics and Astronomy, University of Leicester, Leicester, LE1 7RH, UK [42]NASA Marshall Space Flight Center, Huntsville, AL 35805 [43]Department of Physical Science and Hiroshima Astrophysical Science Center, Hiroshima University, Higashi-Hiroshima 739-8526, Japan [44]University of Maryland, College Park, MD 20742 [45]Centre for Astrophysics Research, University of Hertfordshire, College Lane, Hatfield AL10 9AB , UK [46]European Organization for Nuclear Research (CERN), Geneva, Switzerland [47]Cosmic Radiation Laboratory, Institute of Physical and Chemical Research (RIKEN), Wako, Saitama 351-0198, Japan [48]Centre d'Étude Spatiale des Rayonnements, CNRS/UPS, BP 44346, F-30128 Toulouse Cedex 4, France [49]Orbital Network Engineering, 10670 North Tantau Avenue, Cupertino, CA 95014 [50]University College Dublin, Belfield, Dublin 4, Ireland [51]Istituto Nazionale di Fisica Nucleare, Sezione di Roma "Tor Vergata", I-00133 Roma, Italy [52]Department of Physics and Astronomy, University of Denver, Denver, CO 80208 [53]Institute of Space and Astronautical Science, JAXA, 3-1-1 Yoshinodai, Sagamihara, Kanagawa 229-8510, Japan [54]Department of Physics, Graduate School of Science, University of Tokyo, 7-3-1 Hongo, Bunkyo-ku, Tokyo 113-0033, Japan [55]UCO/Lick Observatories, Santa Cruz, CA 95064 [56]Current address: Sterrenkundig Institut "Anton Pannekoek", 1098 SJ Amsterdam, Netherlands [57]Institut de Ciencies de l'Espai (IEEC-CSIC), Campus UAB, 08193 Barcelona, Spain [58]Kavli Institute for Cosmological Physics, University of Chicago, Chicago, IL 60637 [59]Space Sciences Division, NASA Ames Research Center, Moffett Field, CA 94035-1000 [60]NYCB Real-Time Computing Inc., Lattingtown, NY 11560-1025 [1]Department of Chemistry and Physics, Purdue University Calumet, Hammond, IN 46323-2094 [2]INAF Osservatorio Astronomico di Brera, I-23807 Merate, Italy [63] Institució Catalana de Recerca i Estudis Avançats (ICREA), Barcelona, Spain [64]Consorzio Interuniversitario per la Fisica Spaziale (CIFS), I-10133 Torino, Italy [65]NASA Postdoctoral Program Fellow [66]Dipartimento di Fisica, Università di Roma "Tor Vergata", I-00133 Roma, Italy [67]Joint Center for Particle Nuclear Physics and Cosmology (J-CPNPC), Nanjing 210093, China [68]Purple Mountain Observatory, Chinese Academy of Sciences, Nanjing 210008, China [69]School of Pure and Applied Natural

Sciences, University of Kalmar, SE-391 82 Kalmar, Sweden

Fig. 1. Lightcurves for GRB 080916C observed with the GBM and the LAT, from lowest to highest energies. The energy ranges for the top two panels are chosen to avoid overlap. The top three panels represent the background-subtracted lightcurves for the NaI, the BGO and the LAT. The top panel shows the sum of the counts, in the 8-260 keV energy band, of two NaI detectors (3 and 4). The second is the corresponding plot for BGO detector 0, between 260 keV and 5 MeV. The third shows all LAT events passing the onboard event filter for gamma-rays. The inset panels give a view of the first 15 s from the trigger time. In all cases, the bin width is 0.5s; the per-second counting rate is reported on the right for convenience.

Fig. 2. (Top) Count spectrum for NaI, BGO and LAT in time bin (b): the data points have 1σ error bars while upper-limits are 2σ. The histograms show the number of counts obtained by folding the photon model through the instrument response models. Spectra for time intervals (a) - (e) over the entire energy fit range are available in Figures S1 through S5. (Bottom) The model spectra in νF_ν units for all five time intervals, in which a flat spectrum would indicate equal energy per decade of photon energy, and the changing shapes show the evolution of the spectrum over time. The curves end at the energy of the highest-energy photon observed in each time interval.

Fig. 3. Fit parameters for the Band function, α, β and $E_{\rm peak}$ as a function of time.

Fig. 4. Fluxes (top panel) for the energy range 50–300 keV (shown in blue open squares) and above 100 MeV (red filled squares), and power-law index as a function of the time from T_0 to T_0+1400 s (bottom panel, LAT data only). The red points are obtained by spectral fits of the LAT-only data for all time intervals. The blue points are obtained with the Band functions listed in Table 1 for the first 5 intervals and a power-law fit with index −1.90 ±0.05 for the 6th interval.

Fig. 5. The minimum Lorentz factor $\Gamma_{\rm min}$ as a function of redshift z for two different pulses in the γ-ray light curve. The value of $\Gamma_{\rm min}$, defined by the condition that the γ-ray absorption opacity $\tau_{\gamma\gamma} = 1$, is derived for 3 GeV and 13 GeV photons and variability timescales $\Delta t = 2.0$ s and 20 s in time bins b and d, respectively.

Fig. 6. Low and high-energy gamma-ray fluences of three GRBs observed with both *Fermi* instruments. Both energy ranges are two decades. The diagonal lines indicate constant ratios between the two fluences: dashed: LAT and GBM fluences are equal, dotted: LAT fluence is 10% of GBM fluence, dot-dash: LAT fluence is 1% of GBM fluence.

Table 1. Fit parameters for the Band function, A, α, β and E_{peak} as a function of time. Uncertainties are statistical in nature; the maximum possible systematic errors on the parameter values are comparable to their statistical errors (online supporting material). Times are relative to trigger time T_0 = 00:12:45.613542 UT.

Time bin & Range (s)	A (γ cm^{-2} s^{-1} keV^{-1})	α	β	E_{peak} (keV)	Flux 50-300 keV (γ cm^{-2} s^{-1})	Flux 100 MeV-10 GeV (γ cm^{-2} s^{-1})
a: 0.004 to 3.58	$(55 \pm 2) \times 10^{-3}$	−0.58 ±0.04	−2.63 ±0.12	440 ±27	6.87 ± 0.12	$(2.5 \pm 1.6) \times 10^{-4}$
b: 3.58 to 7.68	$(35 \pm 1) \times 10^{-3}$	−1.02 ±0.02	−2.21 ±0.03	1170 ±140	5.63 ± 0.09	$(4.8 \pm 0.6) \times 10^{-3}$
c: 7.68 to 15.87	$(21 \pm 1) \times 10^{-3}$	−1.02 ±0.04	−2.16 ±0.03	590 ±80	2.98 ± 0.06	$(1.7 \pm 0.2) \times 10^{-3}$
d: 15.87 to 54.78	$(19.4 \pm 0.7) \times 10^{-3}$	−0.92 ±0.03	−2.22 ±0.02	400 ±26	2.44 ± 0.03	$(7.1 \pm 0.9) \times 10^{-4}$
e: 54.78 to 100.86	$(5.2 \pm 0.9) \times 10^{-3}$	−1.05 ±0.10	−2.16 ±0.05	230 ±57	0.54 ± 0.02	$(1.5 \pm 0.4) \times 10^{-4}$

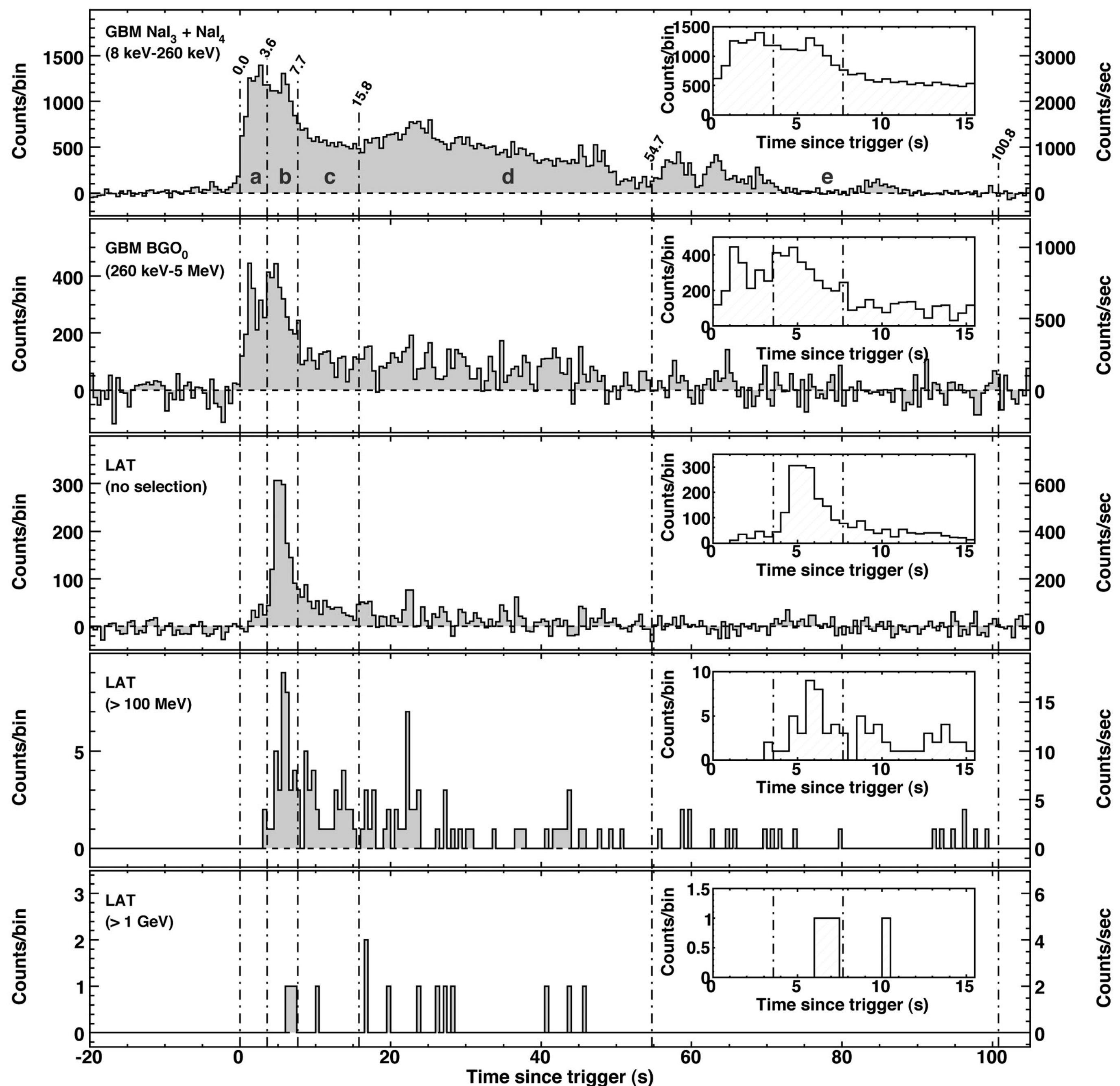

GBM NaI$_3$ + NaI$_4$
(8 keV-260 keV)
GBM BGO$_0$
(260 keV-5 MeV)
LAT
(no selection)
LAT
(> 100 MeV)
LAT
(> 1 GeV)
0.0
3.6
7.7
15.8
54.7
100.8
a
b
c
d
e
Counts/bin
Counts/sec
Time since trigger (s)

A

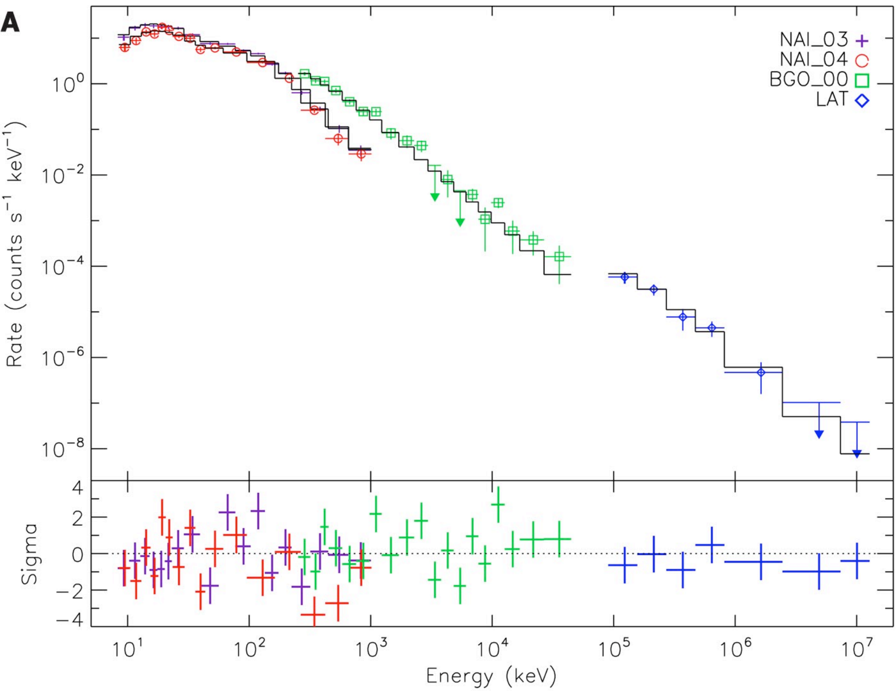

NAI_03
NAI_04
BGO_00
LAT
Rate (counts s^{-1} keV^{-1})
10^0
10^{-2}
10^{-4}
10^{-6}
10^{-8}
Sigma
4
2
0
−2
−4
10^1
10^2
10^3
10^4
10^5
10^6
10^7
Energy (keV)

B

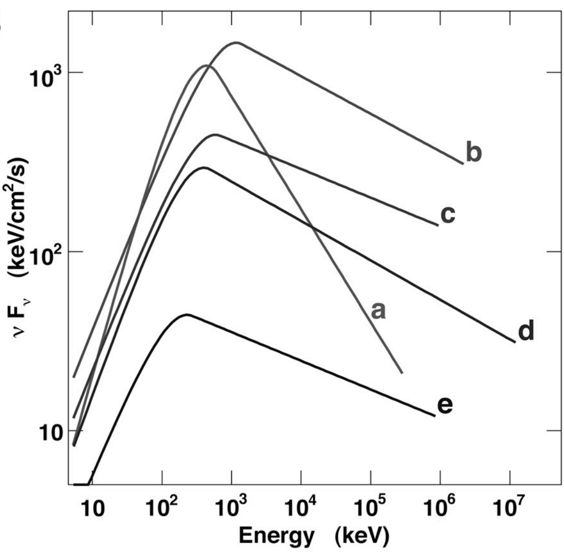

νF_ν (keV/cm^2/s)
10^3
10^2
10
a
b
c
d
e
10
10^2
10^3
10^4
10^5
10^6
10^7
Energy (keV)

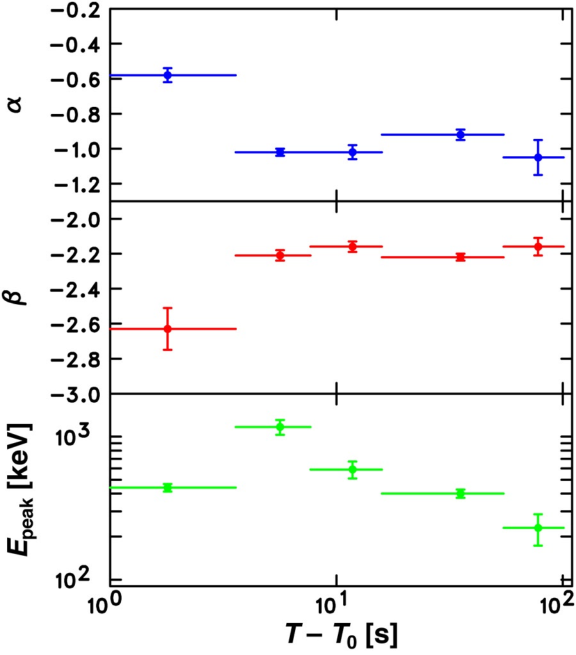

−0.2
−0.4
−0.6
−0.8
−1.0
−1.2
α
−2.0
−2.2
−2.4
−2.6
−2.8
−3.0
β
10^3
10^2
E_{peak} [keV]
10^0
10^1
10^2
$T - T_0$ [s]

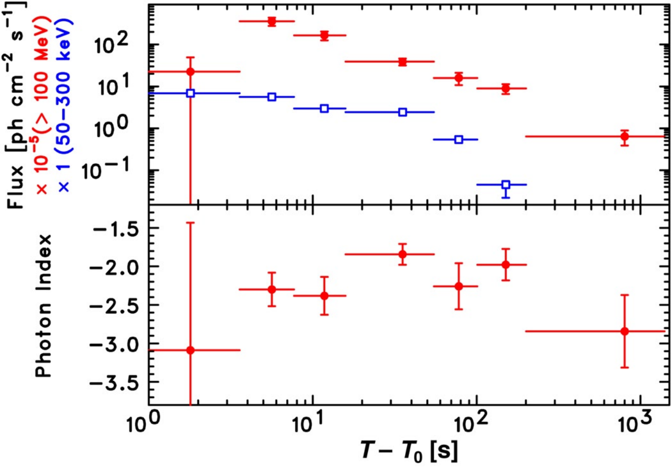

Flux [ph cm^{-2} s^{-1}]
× 10^{-5} (> 100 MeV)
× 1 (50−300 keV)
10^2
10^1
10^0
10^{-1}
Photon Index
−1.5
−2.0
−2.5
−3.0
−3.5
10^0
10^1
10^2
10^3
$T - T_0$ [s]

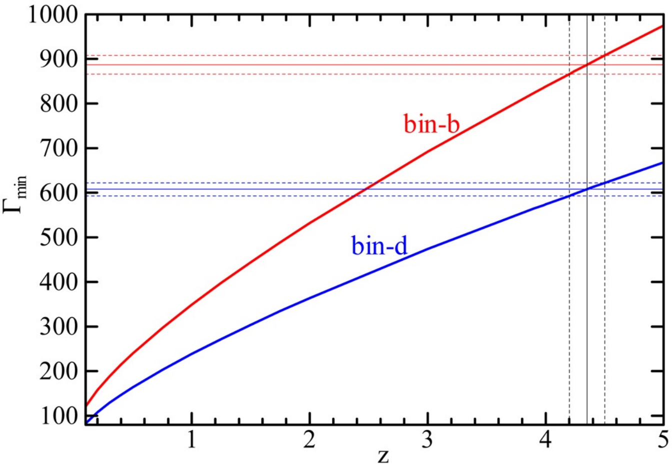
1000
900
800
700
600
500
400
300
200
100
Γ_{min}
1
2
3
4
5
z
bin-b
bin-d

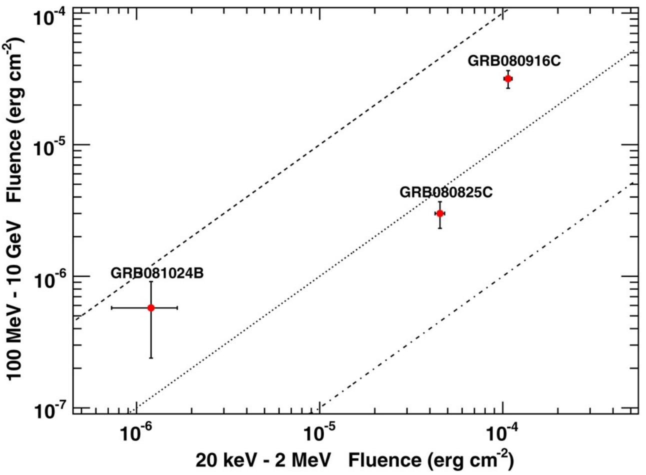
GRB080916C
GRB080825C
GRB081024B
100 MeV - 10 GeV Fluence (erg cm^{-2})
20 keV - 2 MeV Fluence (erg cm^{-2})
10^{-4}
10^{-5}
10^{-6}
10^{-7}